rp-process weak-interaction mediated rates of waiting-point nuclei

Jameel-Un Nabi[1]

Abstract Electron capture and positron decay rates are calculated for neutron-deficient Kr and Sr waiting point nuclei in stellar matter. The calculation is performed within the framework of pn-QRPA model for rp-process conditions. Fine tuning of particle-particle, particle-hole interaction parameters and a proper choice of the deformation parameter resulted in an accurate reproduction of the measured half-lives. The same model parameters were used to calculate stellar rates. Inclusion of measured Gamow-Teller strength distributions finally led to a reliable calculation of weak rates that reproduced the measured half-lives well under limiting conditions. For the rp-process conditions, electron capture and positron decay rates on ^{72}Kr and ^{76}Sr are of comparable magnitude whereas electron capture rates on ^{78}Sr and ^{74}Kr are 1–2 orders of magnitude bigger than the corresponding positron decay rates. The pn-QRPA calculated electron capture rates on ^{74}Kr are bigger than previously calculated. The present calculation strongly suggests that, under rp-process conditions, electron capture rates form an integral part of weak-interaction mediated rates and should not be neglected in nuclear reaction network calculations as done previously.

Keywords electron capture; positron decay; pn-QRPA; rp-process; X-ray bursts; waiting point nuclei

Jameel-Un Nabi

Faculty of Engineering Sciences, GIK Institute of Engineering Sciences and Technology, Topi 23640, Swabi, Khyber Pakhtunkhwa, Pakistan
email: jameel@giki.edu.pk

[1]The Abdus Salam ICTP, Strada Costiera 11, 34014, Trieste, Italy

1 Introduction

At low temperatures ($T_9 \leq 0.3$K), energy generation and accompanying nucleosynthesis in explosive hydrogen burning are characterized by the hot CNO cycles and at higher temperatures by the rp- and the αp-processes (see for example (1)). Recent studies (e.g. (2)) have pointed toward extreme hydrogen burning where at sufficiently high temperature ($T_9 \leq 0.8$K) and density conditions ($\rho \geq 10^4$ gcm^{-3}), depending on the time scale of the explosive event, the rp- and the αp-processes reaction path may well proceed beyond mass A =64 and Z = 32.

The rp-process is characterized by proton capture reaction rates that are orders of magnitude faster than any other competing process, specially β-decay rates. The reaction path follows a series of fast (p,γ)-reactions until further proton capture is inhibited, either by negative proton capture Q-values (proton decay) or small positive proton capture Q-values (photodisintegration). Now the reaction flow has to wait for the relatively slow β-decay and the respective nucleus is hence called a waiting point. It is primarily the reliable estimate of half-lives of the waiting point nuclei that ultimately determine the timescale of the nucleosynthesis process and the produced isotopic abundances. The rp-process produces rapid nucleosynthesis on the proton-rich side of stability line toward heavier proton-rich nuclei. Such processes typically occur when hydrogen fuel is ignited under highly degenerate conditions in explosive events on the surface of compact objects like white dwarfs (novae) and neutron stars (X-ray bursts).

Type I X-ray bursts have been pointed out as possible sites for high temperature hydrogen burning via the rp-process (3). The X-ray bursts are typically generated by a thermonuclear runaway in the hydrogen-rich environment of an accreting compact object fed from a binary companion. The timescale for the thermal runaway ranges from 10–100 s (2). Within this

timescale, the rp-process may proceed well beyond ^{56}Ni (2). Previous attempts to extend the network calculations beyond Z = 32 suffered considerably due to lack of reliable nuclear physics data (3). It was pointed out by authors in Ref. (3) that important parameters for a successful rp-process nucleosynthesis calculation include nuclear masses, nuclear deformations (specially in the regime A = 70–80 because of the wide variety of nuclear shapes displayed in the region) and finally the reliable calculation of stellar electron capture and β-decay rates of the waiting point nuclei along a given reaction path since they determine time structure and abundance patterns.

This article reports on the microscopic calculation of weak-interaction mediated rates (electron capture and β-decay rates) on waiting point nuclei ^{72,74}Kr and ^{76,78}Sr. (It is to be noted that in a true sense only the even-even $N = Z$ nuclei, ^{72}Kr and ^{76}Sr, act as waiting point nuclei because the next nucleus in the proton-capture chain is proton unbound. However, at times, the deformed isotopes, ^{74}Kr and ^{78}Sr, are also considered as waiting point nuclei in literature (see e.g. (4)). It is in this sense that ^{72,74}Kr and ^{76,78}Sr are termed as waiting point nuclei in this manuscript.) The nuclear model chosen to perform this task is the proton-neutron quasiparticle random phase approximation (pn-QRPA) which has a proven track-record for the calculation of electron capture and β-decay rates. Half-lives of β^- decays were calculated systematically for about 6000 neutron-rich nuclei between the beta stability line and the neutron drip line using the pn-QRPA model (5). Similarly half-lives for β^+/EC (electron capture) decays for neutron-deficient nuclei with atomic numbers Z = 10 - 108 were calculated up to the proton drip line for more than 2000 nuclei using the same model (6). These microscopic calculations gave a remarkably good agreement with the then existing experimental data (within a factor of two for more than 90% (73%) of nuclei with experimental half-lives shorter than 1 s for β^- (β^+/EC) decays). Most nuclei of interest of astrophysical importance are the ones far from stability and one has to rely on theoretical models to estimate their beta decay properties. The accuracy of the pn-QRPA model increases with increasing distance from the β-stability line (shorter half-lives) (5; 6). This is a promising feature with respect to the prediction of experimentally unknown half-lives (specially those present in the stellar interior), implying that the predictions are made on the basis of a realistic physical model. Later Nabi and Klapdor-Kleingrothaus reported the calculation of weak-interaction rates for more than 700 nuclei with A = 18 to 100 in stellar environment using the same nuclear model (7). These included capture rates, decay rates, gamma heating rates, neutrino energy loss rates, probabilities of beta-delayed particle emissions and energy rate of these particle emissions. The authors then presented a detailed calculation of stellar weak-interaction rates over a wide range of temperature and density scale for sd- (8) and fp/fpg-shell nuclei (9). Since then these calculations were further refined with use of more efficient algorithms, computing power, incorporation of latest data from mass compilations and experimental values, and fine-tuning of model parameters both in the sd- shell (e.g. (10)) and fp-shell nuclei (e.g. (11)).

The next section discusses the calculation of stellar weak-interaction mediated rates using the pn-QRPA formalism. The calculated Gamow-Teller strength distributions of waiting point nuclei ^{72,74}Kr and ^{76,78}Sr are also presented in this section. The rp-process electron capture and positron decay rates are presented and compared with previous calculations in Section 3. Summary and conclusions finally follow in Section 4.

2 Description of the microscopic model

The microscopic calculation of Gamow-Teller strength distributions under stellar conditions is a challenging task. The calculations become more challenging as the number of nucleons increases. Out of the very limited available options, the pn-QRPA model can handle any arbitrarily heavy system of nucleons and performs a microscopic calculation of ground and excited state Gamow-Teller strength functions (12; 13).

For the present pn-QRPA calculation single particle energies and wave functions were calculated in the Nilsson model (14), which takes into account nuclear deformations. Pairing was treated in the BCS approximation. The proton-neutron residual interactions occur in two different forms, namely as particle-hole and particle-particle interactions. These interactions were given separable form and were characterized by two interaction constants χ and κ, respectively. These parameters are regarded as the two most important model parameters in the pn-QRPA theory (see Refs. (5; 6)). In this work a fine tuning of these parameters was done which optimally reproduced the measured half-lives for ^{72,74}Kr and ^{76,78}Sr (for measured half-lives see Refs. (15; 16; 17)). The particle-hole-interaction parameter, χ, is known to influence the calculated position of the Gamow-Teller giant resonance (GTGR). Normally for the case of stable nuclei, the constant χ is parameterized such that the experimentally observed energy of the GTGR is reproduced in the best way. However Hirsch and collaborators (6), using the pn-QRPA model, deduced the locally best χ values for individual isotopic chains. It was shown in (6) that larger

values of χ always shift GTGR to higher excitation energy but the shift caused by a small change of χ does not result in the same energetic shift for all isotopes. On the other hand, the particle-particle-interaction (κ) is known to enhance the ground-state correlations and leads to a redistribution of the calculated β strength (and is therefore related to the half-lives of the nuclei), which is commonly shifted to lower excitation energies (6). Again, rather than going for a parameterization of κ, the local best value for an isotopic chain that best reproduces the measured half-lives, was chosen in this work. Fixing the interaction constants, χ and κ, in this way led to considerable improvement in the accuracy of the pn-QRPA calculation (5; 6; 8; 9). For details of choosing the locally best values of the strength parameters see Ref. (6). The chosen values of χ were 0.27 MeV and 0.36 MeV for Kr and Sr isotopes, respectively. The corresponding κ values were 0.045 Mev and 0.044 MeV, respectively.

The deformation parameter was recently argued as an important parameter for QRPA calculations at par with the pairing parameter by Stetcu and Johnson (18). To make the problem more challenging the nuclei in the mass region considered for this work are known to have coexistence of prolate and oblate shapes. For ^{72}Kr the deformation parameter was calculated using the mass formula of Ref. (19). The chosen value of -0.2647 is also in line with the findings of authors in Ref. (15; 20) which favor an oblate shape for ^{72}Kr. For the case of ^{74}Kr and ^{78}Sr, the experimentally adopted values of the deformation parameters, extracted by relating the measured energy of the first 2^+ excited state with the quadrupole deformation, were available and taken from Raman et al. (21). The deformation parameter for the case of ^{76}Sr was again taken from the mass formula of Ref. (19) in close agreement with the findings of Nácher and collaborators (22). Table 1 shows the chosen values of nuclear deformations used in the model and the calculated half-lives for the waiting point nuclei. All half-lives are given in units of *sec*. Measured values are given in third column whereas the pn-QRPA calculated terrestrial half-lives of Kr and Sr isotopes are given in fourth column. The calculated terrestrial half-lives have dominant contribution from positron (β^+) decay rates. Since the chosen values of χ and κ reproduced the measured half-lives fairly well, no quenching factor was introduced in the present calculation. The last column compares the pn-QRPA calculated stellar half-lives with the terrestrial ones under limiting conditions. At the lowest temperature considered in this work (T = 10^7 K), excited parent states are not appreciably populated, while at the lowest density considered in this work ($\rho Y_e = 10^{0.5}$ gcm^{-3}), the continuum electron density is quite low. It is to be noted that ρ stands for the baryon density whereas Y_e is the ratio of the lepton number to the baryon number and their product ρY_e implies the electron density and is simply referred to as density throughout this manuscript. Except for electron capture, the stellar rates should be close to the terrestrial values. The exception arises because only continuum electron capture and no bound-states capture is calculated. Again, for the stated physical conditions, the continuum electron capture rates are orders of magnitude smaller than the corresponding positron (β^+) decay rates. As can be seen the comparison is satisfactory. Nuclear masses and Q-values required for the calculation were taken from the mass compilation of Audi et al. (23). The same set of model parameters were used to calculate electron capture and positron decay rates for these waiting point nuclei under rp-process conditions.

The electron capture (ec) and positron decay (pd) rates of a transition from the i^{th} state of the parent to the j^{th} state of the daughter nucleus are given by

$$\lambda_{ij}^{ec(pd)} = \left[\frac{\ln 2}{D}\right]\left[B(F)_{ij} + \left(g_A/g_V\right)^2 B(GT)_{ij}\right] \left[f_{ij}^{ec(pd)}(T, \rho Y_e, E_f)\right]. \quad (1)$$

The value of D was taken to be 6295s (24). B(F) and B(GT) are reduced transition probabilities of the Fermi and Gamow-Teller (GT) transitions, respectively,

$$B(F)_{ij} = \frac{1}{2J_i+1} \mid< j \parallel \sum_k t_\pm^k \parallel i >\mid^2 . \quad (2)$$

$$B(GT)_{ij} = \frac{1}{2J_i+1} \mid< j \parallel \sum_k t_\pm^k \vec{\sigma}^k \parallel i >\mid^2 . \quad (3)$$

Here $\vec{\sigma}^k$ is the spin operator and $t_\pm^k$ stands for the isospin raising and lowering operator with (g_A/g_V) = -1.254 (25). Details of the calculation of reduced transition probabilities (for both ground state and excited states GT transitions) can be found in Ref. (8).

The $f_{ij}^{ec(pd)}$ are the phase space integrals and are functions of stellar temperature (T), electron density (ρY_e) and Fermi energy (E_f) of the electrons. They are explicitly given by

$$f_{ij}^{ec} = \int_{w_l}^{\infty} w\sqrt{w^2-1}(w_m + w)^2 F(+Z, w) G_- dw. \quad (4)$$

and by

$$f_{ij}^{pd} = \int_{1}^{w_m} w\sqrt{w^2-1}(w_m - w)^2 F(-Z, w)(1-G_+) dw, \quad (5)$$

In Eqs. (4) and (5), w is the total energy of the electron including its rest mass. w_m is the total β-decay energy,

$$w_m = m_p - m_d + E_i - E_j, \tag{6}$$

where m_p and E_i are masses and excitation energies of the parent nucleus, and m_d and E_j of the daughter nucleus, respectively. F($\pm$ Z,w) are the Fermi functions and were calculated according to the procedure adopted by Gove and Martin (26). $G_\pm$ are the Fermi-Dirac distribution functions for positrons (electrons).

$$G_+ = \left[\exp\left(\frac{E+2+E_f}{kT}\right)+1\right]^{-1}, \tag{7}$$

$$G_- = \left[\exp\left(\frac{E-E_f}{kT}\right)+1\right]^{-1}, \tag{8}$$

here E is the kinetic energy of the electrons and k is the Boltzmann constant.

The total capture/decay rate per unit time per nucleus is finally given by

$$\lambda^{ec(pd)} = \sum_{ij} P_i \lambda_{ij}^{ec(pd)}, \tag{9}$$

where P_i is the probability of occupation of parent excited states and follows the normal Boltzmann distribution. After the calculation of all partial rates for the transition $i \rightarrow j$ the summation was carried out over 300 initial and final states and satisfactory convergence was achieved in the rate calculation. These 300 excited states were chosen with an appropriate bandwidth covering energies up to 10 MeV in parent and 20 MeV in daughter nuclei.

In order to ensure a reliable set of calculated rates three important steps were undertaken in this calculation: (i) all available experimental (XUNDL) data were incorporated in the calculation; (ii) all available measured GT strength distribution were inserted in the calculation wherever the theory was missing them, and (iii) all excited state GT strength functions were microscopically calculated within the pn-QRPA framework. The theoretical excitation energy of a low-lying level was replaced by the observed excitation energy if this experimental level had a definite spin-parity assignment and was located within 0.5 MeV of the theoretically calculated level. If more than one theoretically calculated energy eigenvalue falls within 0.5 MeV of a measured level then the replacement was done for the level lying closest to the measured value. If there appeared a level without definite spin and/or parity assignment in the sequence of experimental levels from the ground state to higher excited levels, no replacement of theoretical levels with measured levels was done beyond this excitation energy. The calculated B(GT) value was then replaced by the observed B(GT) value (if available) when the calculated energies of the parent and daughter levels were replaced by the experimental energies. Missing measured states were inserted and inverse transitions (along with their logft values) were also incorporated in the calculation. If the relevant transition was not measured but the inverse transition was measured, the deduced observed B(GT) value using this inverse transition was used in this calculation. The measured B(GT_+) strength distribution of ^{72}Kr from Ref. (15), of ^{74}Kr from Ref. (27) and of ^{78}Sr from Ref. (22) were inserted in the calculation. As mentioned earlier the pn-QRPA model has the additional advantage that all excited state GT strength functions are calculated in a microscopic fashion and the so-called Brink's hypothesis is not assumed in this calculation. Brink's hypothesis states that GT strength distribution on excited states is *identical* to that from ground state, shifted *only* by the excitation energy of the state. Recent pn-QRPA calculations (e.g. (12; 13)) have shown Brink's hypothesis to be a poor approximation to be used in calculation of stellar weak rates specially at high temperatures and densities. These steps ensured a reliable set of calculation of ground and excited state GT strength distributions to be later used for the calculation of weak rates for waiting point nuclei.

Fig. 1 shows the calculated BGT_+ distributions for the Kr and Sr isotopes up to 20 MeV in daughter nuclei. As can be seen from Fig. 1, the GT distributions are well fragmented and extend up to high excitation energies in daughter nuclei. The model independent Ikeda sum rule was satisfied in the calculation. The discussion on the calculated weak rates follows in the next section.

3 Thermal electron capture and positron decay rates of waiting point nuclei

The calculated Fermi and GT strength distributions, along with the corresponding phase space calculations were inserted into Eq. (1) for the calculation of partial rates. The calculated partial rates were finally added through the recipe of Eq. (9) to get the total stellar electron capture and positron decay rates. The calculated rates for Kr and Sr isotopes are shown in Fig. 2 and Fig. 3, respectively.

The left panels of Fig. 2 and Fig. 3 depict the calculated electron capture and positron decay rates, separately, as a function of stellar temperature and density. The electron capture rates are calculated at densities

$\rho Y_e = 10^5, 10^6, 10^{6.5}, 10^7$ and 10^8 gcm^{-3}. T_9 gives the stellar temperature in units of 10^9 K. The calculation is performed up to $T_9 = 30$. It is to be noted that such high temperatures are far away from the relevant range of temperatures for the rp-process. Nevertheless the calculation was performed till $T_9 = 30$ in order to study the evolution of rates with increasing stellar temperatures. The right columns in both figures show the sum of calculated electron capture and positron decay rates at the respective temperature and density points. The left panels show that the calculated positron decay rates are almost independent of stellar densities. It can be seen from the upper left panel of Fig. 2 that at low stellar temperatures ($T_9 \leq 4$K) and densities ($\rho Y_e \leq 10^{6.5}$ gcm^{-3}), the positron decay rates of ^{72}Kr are bigger than the electron capture rates by as much as a factor of 23. According to studies by authors in Ref. (3; 2) the peak conditions for rp-process are in the vicinity of $T_9 = 1$–3 K and $\rho Y_e = 10^6 - 10^7$ gcm^{-3}. It can be seen from the current calculation that electron capture and positron decay rates of ^{72}Kr contribute roughly equally to the total weak rates at rp-process conditions. However at high temperatures and densities the electron capture rates shoot up and are bigger by more than two orders of magnitude than the corresponding positron decay rates. For the case of ^{74}Kr the electron capture rates are always bigger than the positron decay rates (lower left panel of Fig. 2). The electron capture rates are more than 1–2 orders of magnitude bigger than positron decay rates for rp-process conditions and the total rates are commanded by the electron capture rates (lower right panel). For still higher temperatures and densities the positron decay rates are almost 3 orders of magnitude smaller and can safely be neglected as compared to electron capture rates.

Fig. 3 shows the calculated weak-interaction mediated rates for ^{76,78}Sr. The upper panels are for ^{76}Sr and the lower for ^{78}Sr. Akin to the case of ^{72}Kr, at low stellar temperatures ($T_9 \leq 4.5$K) and densities ($\rho Y_e \leq 10^6$ gcm^{-3}), the positron decay rates dominate and are as much as a factor 17 bigger than the corresponding electron capture rates. At high temperatures and densities the electron capture rates shoot exponentially due to increase in phase space factors and are more than two orders of magnitude bigger. For the rp-process conditions the situation is interesting. At density $\rho Y_e = 10^6$ gcm^{-3} the positron decay rates are a factor 2–3 bigger, at $\rho Y_e = 10^{6.5}$ gcm^{-3} the two rates are of comparable magnitude while at $\rho Y_e = 10^7$ gcm^{-3} the electron capture rates are a factor 4 bigger. At high temperatures and densities the total weak rates are driven by electron capture rates (upper right panel of Fig. 3). For the case of ^{78}Sr the positron decay rates are bigger than the electron capture rates by as much as a factor of 7 at low temperatures ($T_9 \leq 3.5$K) and density ($\rho Y_e \leq 10^{5.5}$ gcm^{-3}) conditions. For the rp-process conditions the two rates are of equal magnitude at $\rho Y_e = 10^6$ gcm^{-3} whereas the electron capture rates are bigger by a factor of 3–10 at $\rho Y_e = 10^{6.5} - 10^7$ gcm^{-3}. Once again at high temperatures the electron capture rates are bigger by more than two orders of magnitude as expected.

The contribution of parent excited states to the total electron capture and positron decay rates is shown in Table 2. The analysis was done at the selected stellar density of $\rho Y_e = 10^{6.5}$ gcm^{-3} (a typical value for rp-conditions). Shown also in Table 2 are the ground state electron capture and positron decay rates and the ratios of the ground state capture rate to total electron capture rate ($R_{ec}(G/T)$) and ground state decay rate to total positron decay rate ($R_{pd}(G/T)$) for the waiting point nuclei. For the selected density scale no significant contribution comes to the total decay rates from parent excited states whereas at $T_9 = 30$K the excited states contribute roughly 95% to the total capture rates. It is to be noted that this analysis can change appreciably for higher stellar densities.

Fig. 4 displays the half-lives (including both the positron decay and electron capture contributions), as a function of stellar temperatures at a selected density of $\rho Y_e = 10^{6.5}$ gcm^{-3} for Sr and Kr waiting point nuclei. Again the calculation is performed up to $T_9 = 30$K for reasons mentioned above. The calculated half-lives decrease as stellar temperature increases as expected since the electron capture rates increases substantially with increasing temperatures (see Fig. 2 and Fig. 3). It is to be noted that for rp-process conditions the half-lives decrease very mildly. For higher temperature the fall in half-lives is rather steep.

The calculated rates were also compared with the calculation of weak-interaction rates for Kr and Sr isotopes by Sarriguren (4). The same author later expanded his calculation for waiting point nuclei extending from Ni to Sn (28). Sarriguren used quasiparticle basis corresponding to a deformed self-consistent Skyrme Hartee-Fock calculation with SLy4 (29) force. Pairing correlations were treated in BCS formalism. The spin-isospin interactions were considered both in particle-hole and particle-particle channel and wavefunctions were calculated using the Bohr-Mottelson factorization (30). Sarriguren used a quenching factor of 0.55 in his calculation. The pn-QRPA calculated electron capture rates are in good agreement with Sarriguren's rate except for the case of ^{74}Kr. The pn-QRPA positron decay rates are bigger specially at high temperatures by as much as a factor of 40.

Table 3 compares the weak-interaction rates and calculated half-lives for Kr isotopes at $\rho Y_e = 10^6$ gcm^{-3}. In the table $R_{ec}(N/S)$, $R_{pd}(N/S)$ and $R_{hl}(N/S)$ denote the ratio of pn-QRPA calculated electron capture (ec), positron decay (pd) and half-lives (hl), respectively, to those calculated by Sarriguren. It can be seen from Table 3 that the calculated electron capture rates on ^{72}Kr are in reasonable agreement with those of Sarriguren. Positron decay rates of ^{72}Kr are also in reasonable agreement except at $T_9 = 10$K where reported rates are around a factor 5 bigger. Sarriguren did not calculate weak-interaction rates for $T_9 > 10$K. The last column shows the ratio of the pn-QRPA calculated total half-lives (including electron capture and positron decay) to those calculated by Sarriguren. The comparison of total half-lives for ^{72}Kr is correspondingly fairly good. Only at high temperatures is the pn-QRPA calculated half life roughly half that reported by Sarriguren. The origin of this difference might be connected to the fact that energy levels beyond 1 MeV were not considered in Sarriguren's calculation. These high-lying energy states have a finite occupation probability at high temperatures and resulted in a much bigger total weak rate. Much bigger differences are seen for the case of weak rates for ^{74}Kr. The reported electron capture rates on ^{74}Kr are a factor 3–7 bigger whereas positron decay rates are almost double at low temperatures and around a factor 30 bigger at $T_9 = 10$K. The total weak rates are around an order of magnitude bigger and consequently the calculated half-lives are roughly an order of magnitude smaller. The reason for this difference could be attributed to the different calculation of the GT distributions in the two models. The pn-QRPA model calculated a total B(GT) value of 10.73, up to 20 MeV, with the centroid lying around 5.10 MeV in ^{74}Br (see Fig. 1). The pn-QRPA calculated total B(GT) strength value and/or placement of GT centroid can lead to enhancements in reported rates.

A better comparison of reported calculation with that of Sarriguren is seen for the case of Sr isotopes (Table 4). For ^{76}Sr the electron capture and positron decay rates are in reasonable agreement. The calculated half-lives also agree fairly well except at $T_9 = 10$K when the reported positron decay rate on ^{76}Sr is around a factor 4 bigger. The comparison of electron capture rates on ^{78}Sr is reasonable. The pn-QRPA reported positron decay rates are double the Sarriguren's rate at low temperatures and around factor 10 –40 bigger at higher temperatures. For the rp-process conditions the pn-QRPA calculated electron capture rates on ^{76}Sr (^{78}Sr) are slightly bigger (smaller) and positron decay rates for ^{76}Sr (^{78}Sr) are slightly smaller (bigger) than the corresponding Sarriguren rates. The calculated half-lives of Sr isotopes are in reasonable agreement except at high temperatures when the half-life calculated by Sarriguren is around a factor 1.5 bigger for reasons already mentioned above.

4 Conclusions

To summarize weak-interaction rates for neutron-deficient Kr and Sr isotopes were calculated within the framework of pn-QRPA model. Proper choice of deformation parameter and smart choice of particle-particle and particle-hole interaction terms led to correct reproduction of the measured half-lives. The same model parameters were used to calculate stellar weak rates for rp-process conditions. Whereas electron capture and positron decay rates, of other krypton and strontium isotopes in stellar matter, can be calculated using the same model parameters as stated here, a case by case fitting procedure is required for other isotopic chains within the framework of pn-QRPA model. Measured data were inserted wherever available to increase the reliability of calculated rates. The pn-QRPA reported electron capture rates on ^{74}Kr are around a factor 6 bigger than those calculated by Sarriguren under rp-conditions. The present calculation clearly shows that the electron capture rates are at least of similar magnitude as the competing positron decay rates under rp-process conditions. The calculation provide concrete evidence that for typical rp-process conditions, $T_9 =$ 1–3 K and $\rho Y_e = 10^6 - 10^7$ gcm^{-3}, electron capture rates on ^{72}Kr and ^{76}Sr are of same order of magnitude as the corresponding positron decay rates. On the other hand electron capture rates on ^{78}Sr and ^{74}Kr are 1–2 orders of magnitude bigger than the respective positron decay rates. The study reconfirms the conclusion made by Sarriguren that electron capture rates form an integral part of weak-interaction mediated rates under rp-process conditions and should not be neglected in nuclear reaction network calculations as done in past (e.g. (3)).

Acknowledgments: The author would like to acknowledge the kind hospitality provided by the Abdus Salam ICTP, Trieste, where this project was completed. The author wishes to acknowledge the support of research grant provided by the Higher Education Commission, Pakistan through the HEC Project No. 20-1283. The author also wishes to thank P. Sarriguren, A. Algora, E. Nácher and B. Rubio for useful discussions and for providing data used in this work.

References

Prialnik D. : An Introduction to the theory of stellar structure and evolution. Cambridge University Press, Cambridge. (2000)

Van Wormer L., Görres J., Iliadis C., Wiescher M. and Thielemann F.-K.: Reaction Rates and Reaction Sequences in the rp-process. Astrophys. J. **432**, 326 (1994)

Schatz H., Aprahamian A., Grres J., Wiescher M., Rauscher T., Rembges J. F., Thielemann F.-K., Pfeiffer B., Möller P. , Kratz K.-L., Herndl H., Brown B. A., Rebel H.: rp-process nucleosynthesis at extreme temperature and density conditions. Phys. Rep. **294**, 167 (1998)

Sarriguren P.: Weak interaction rates for Kr and Sr waiting-point nuclei under rp-process conditions. Phys. Lett. B **680**, 438 (2009)

Staudt A., Bender E., Muto K., Klapdor-Kleingrothaus H.V.: Second-Generation Microscopic Predictions of Beta-Decay Half-lives of Neutron-Rich Nuclei. At. Data Nucl. Data Tables **44**, 79 (1990)

Hirsch M., Staudt A., Muto K., Klapdor-Kleingrothaus H.V.: Microscopic Predictions of β^+/EC-Decay Half-Lives. At. Data Nucl. Data Tables **53**, 165 (1993)

Nabi J.-Un, Klapdor-Kleingrothaus H.V.: Microscopic Calculations of Weak Interaction Rates of Nuclei in Stellar Environment for A = 18 to 100. Eur. Phys. J. A **5**, 337 (1999)

Nabi J.-Un, Klapdor-Kleingrothaus H.V.: Weak Interaction Rates of sd-Shell Nuclei in Stellar Environments Calculated in the Proton-Neutron Quasiparticle Random-Phase Approximation. At. Data Nucl. Data Tables **71**, 149 (1999)

Nabi J.-Un, Klapdor-Kleingrothaus H.V.: Microscopic Calculations of Stellar Weak Interaction Rates and Energy Losses for fp- and fpg-Shell Nuclei. At. Data Nucl. Data Tables **88**, 237 (2004)

Nabi J.-Un: Stellar neutrino energy loss rates due to ^{24}Mg for O+Ne+Mg core simulations. Phys. Rev. C**78**, 045801 (2008)

Nabi J.-Un, Rahman M.-Ur.: Gamow-Teller Strength Distributions and Electron Capture Rates for ^{55}Co and ^{56}Ni. Phys. Lett. B **612**, 190 (2005)

Nabi J.-Un.: Stellar $\beta^{\pm}$ decay rates of iron isotopes and its implications in astrophysics. Adv. Space Res. **46**, 1191 (2010)

Nabi J.-Un.: Ground and excited states Gamow-Teller strength distributions of iron isotopes and associated capture rates for core-collapse simulations. Astrophys. Space Sci. **331**, 537 (2011)

Nilsson S.G.: Binding States of Individual Nucleons in Strongly Deformed Nuclei. Mat. Fys. Medd. Dan. Vid. Selsk **29**, 16 (1955)

Piqueras I., *et al.*: Beta-decay of the N = Z nucleus 72Kr. Eur. Phys. J. A **16**, 313 (2003)

Schmeing H., Hardy J.C., Graham R.L., Geiger J.S.: The decay of 74Kr. Nucl. Phys. A**242**, 232 (1975)

Grawe H, Hoff P., Omtvedt J.P., Steffensen K., Eder R., Haas H., Ravn H.: Study of the +/EC decay of the neutron deficient nuclei 76,78Sr and 79Y. Eur. Phys. J. A **341**, 247 (1992)

Stetcu I., Johnson C.W.: Gamow-Teller Transitions and Deformation in the Proton-Neutron Random Phase Approximation. Phys. Rev. C**69**, 024311 (2004)

Möller P., Nix J.R.: Atomic Masses and Nuclear Ground-State Deformations Calculated with a New Macroscopic-Microscopic Model. At. Data Nucl. Data Tables **26**, 165 (1981)

Patra S.K., Praharaj C.R.: Shapes of exotic nuclei in the mass A = 70 region. Phys. Rev. C**47**, 2978 (1993)

Raman S., Malarkey C.H., Milner W.T., Nestor, Jr. C.W., Stelson P.H.: Transition Probability, B(E2)↑, from the Ground to the First-Excited 2^+ State of Even-Even Nuclides. At. Data Nucl. Data Tables **36**, 1 (1987)

Nácher E., *et al.*: Deformation of the N = Z Nucleus 76Sr using β-Decay Studies. Phys. Rev. Lett.**92**, 232501 (2004)

Audi G., Wapstra A.H., Thibault C.: The AME2003 Atomic Mass Evaluation (II). Tables, Graphs and References. Nucl. Phys. A**729**, 337 (2003)

Yost G.P., Barnett R.M., Hinchliffe I., *et al.* (Particle Data Group): Review of Particle Properties. Phys. Lett. **B204**, 1 (1988)

Rodin V., Faessler A., Simkovic F., Vogel P.: Uncertainties in the 0-Decay Nuclear Matrix Elements, Czech. J. Phys **56**, 495 (2006)

Gove N.B., Martin M.J.: Log-F Tables For Beta Decay. At. Data Nucl. Data Tables **10**, 205 (1971)

Poirier E., *et al.*: B(GT) strength from β-decay measurements and inferred shape mixing in 74Kr. Phys. Rev. C**69**, 034307 (2004)

Sarriguren P.: Stellar weak decay rates in neutron-deficient medium-mass nuclei. Phys. Rev. C**83**, 025801 (2011)

Chabanat E., Bonche P., Haensel P., Meyer J., Schaeffer R.: A skyrme parametrization from subnuclear to neutron star densities Part II. Nuclei far from stabilities. Nucl. Phys. A**635**, 231 (1998)

Bohr A., B. Mottelson.: Nuclear Structure, Benjamin, New York. (1975)

This manuscript was prepared with the AAS LaTeX macros v5.2.

Table 1 Comparison of measured and pn-QRPA calculated half-lives in units of *sec*. Nuclear deformations are given in second column. The third and fourth columns give the measured and calculated terrestrial half-lives, respectively. The fifth column gives the limiting values of calculated stellar half-lives at density $10^{0.5} gcm^{-3}$ and temperature $10^7 K$.

Nucleus	Deformation	$T_{1/2}$(exp)	$T_{1/2}$(terr)	$T_{1/2}$(0.5,0.01)
^{72}Kr	-0.2647	17.2	17.2	16.7
^{74}Kr	+0.3870	690	683.8	665.7
^{76}Sr	+0.4074	8.9	8.8	8.53
^{78}Sr	+0.4340	150	154.7	142.95

Table 2 The *ground state* electron and positron decay rates, $\lambda_{ec}(G)$, $\lambda_{pd}(G)$, respectively, for $^{72,74}Kr$ and $^{74,76}Sr$ in units of sec^{-1}. Given also are the ratios of the ground state capture and decay rates to total rate, $R_{ec}(G/T)$, $R_{pd}(G/T)$, respectively. The first column gives the corresponding values of stellar density, ρY_e (gcm^{-3}), and temperature, T_9 (in units of 10^9 K), respectively.

	^{72}Kr			
$(\rho\mathbf{Y_e}, \mathbf{T_9})$	$\lambda_{\mathbf{ec}}(\mathbf{G})$	$\mathbf{R_{ec}(G/T)}$	$\lambda_{\mathbf{pd}}(\mathbf{G})$	$\mathbf{R_{pd}(G/T)}$
($10^{6.5}$,0.01)	3.57E-02	1.00E+00	4.15E-02	1.00E+00
($10^{6.5}$,1)	3.59E-02	1.00E+00	4.15E-02	1.00E+00
($10^{6.5}$,1.5)	3.62E-02	1.00E+00	4.15E-02	1.00E+00
($10^{6.5}$,2)	3.67E-02	1.00E+00	4.15E-02	1.00E+00
($10^{6.5}$,2.5)	3.75E-02	1.00E+00	4.15E-02	1.00E+00
($10^{6.5}$,3)	3.91E-02	1.00E+00	4.15E-02	1.00E+00
($10^{6.5}$,30)	1.48E+01	2.83E-02	2.24E-03	6.69E-04
	^{74}Kr			
($10^{6.5}$,0.01)	4.15E-02	1.00E+00	1.04E-03	1.00E+00
($10^{6.5}$,1)	4.25E-02	1.00E+00	1.04E-03	1.00E+00
($10^{6.5}$,1.5)	4.36E-02	1.00E+00	1.04E-03	1.00E+00
($10^{6.5}$,2)	4.52E-02	1.00E+00	1.04E-03	1.00E+00
($10^{6.5}$,2.5)	4.74E-02	1.00E+00	1.04E-03	1.00E+00
($10^{6.5}$,3)	5.05E-02	1.00E+00	1.04E-03	9.98E-01
($10^{6.5}$,30)	1.16E+01	5.37E-02	3.26E-05	9.61E-05
	^{76}Sr			
($10^{6.5}$,0.01)	9.61E-02	1.00E+00	8.12E-02	1.00E+00
($10^{6.5}$,1)	9.69E-02	1.00E+00	8.12E-02	1.00E+00
($10^{6.5}$,1.5)	9.79E-02	1.00E+00	8.12E-02	1.00E+00
($10^{6.5}$,2)	9.96E-02	1.00E+00	8.12E-02	1.00E+00
($10^{6.5}$,2.5)	1.02E-01	1.00E+00	8.12E-02	1.00E+00
($10^{6.5}$,3)	1.07E-01	1.00E+00	8.12E-02	1.00E+00
($10^{6.5}$,30)	2.36E+01	3.93E-02	4.42E-03	1.23E-03
	^{78}Sr			
($10^{6.5}$,0.01)	1.42E-02	1.00E+00	4.85E-03	1.00E+00
($10^{6.5}$,1)	1.43E-02	1.00E+00	4.85E-03	1.00E+00
($10^{6.5}$,1.5)	1.45E-02	1.00E+00	4.85E-03	1.00E+00
($10^{6.5}$,2)	1.48E-02	1.00E+00	4.85E-03	1.00E+00
($10^{6.5}$,2.5)	1.53E-02	1.00E+00	4.85E-03	1.00E+00
($10^{6.5}$,3)	1.60E-02	1.00E+00	4.84E-03	9.98E-01
($10^{6.5}$,30)	3.59E+00	2.60E-02	1.41E-04	1.77E-04

Table 3 Comparison of electron capture (ec) and positron decay (pd) rates with those calculated by Sarriguren (4) for Kr isotopes. Number in fourth and seventh column gives the ratio of reported rates to the rates calculated by Sarriguren. The last column shows the ratio of the pn-QRPA calculated total half-lives to those calculated by Sarriguren. The rates are compared at stellar density $\rho Y_e = 10^6$ gcm^{-3}.

				^{72}Kr			
	ec			**pd**			
T_9	Nabi	Sarriguren	$R_{ec}(N/S)$	Nabi	Sarriguren	$R_{pd}(N/S)$	$R_{hl}(N/S)$
0.01	1.29E-02	1.62E-02	7.97E-01	4.15E-02	3.47E-02	1.20E+00	9.35E-01
1	1.23E-02	1.54E-02	7.99E-01	4.15E-02	3.48E-02	1.19E+00	9.33E-01
2	1.19E-02	1.55E-02	7.66E-01	4.15E-02	3.99E-02	1.04E+00	1.04E+00
3	1.37E-02	1.92E-02	7.12E-01	4.15E-02	5.07E-02	8.19E-01	1.27E+00
10	1.33E+00	9.61E-01	1.38E+00	3.38E-01	7.52E-02	4.49E+00	6.21E-01
				^{74}Kr			
0.01	1.43E-02	2.20E-03	6.49E+00	1.04E-03	5.48E-04	1.90E+00	1.79E-01
1	1.40E-02	2.20E-03	6.36E+00	1.04E-03	5.79E-04	1.80E+00	1.85E-01
2	1.43E-02	2.66E-03	5.38E+00	1.04E-03	8.78E-04	1.18E+00	2.30E-01
3	1.74E-02	3.65E-03	4.76E+00	1.03E-03	1.12E-03	9.20E-01	2.59E-01
10	1.04E+00	3.32E-01	3.13E+00	4.44E-02	1.44E-03	3.07E+01	3.08E-01

Table 4 Same as Table 3 but for Sr isotopes.

				^{76}Sr			
	ec			**pd**			
T_9	Nabi	Sarriguren	$R_{ec}(N/S)$	Nabi	Sarriguren	$R_{pd}(N/S)$	$R_{hl}(N/S)$
0.01	3.45E-02	3.04E-02	1.13E+00	8.12E-02	9.28E-02	8.75E-01	1.06E+00
1	3.31E-02	2.99E-02	1.11E+00	8.12E-02	9.95E-02	8.16E-01	1.13E+00
2	3.22E-02	3.04E-02	1.06E+00	8.12E-02	1.14E-01	7.10E-01	1.28E+00
3	3.72E-02	3.55E-02	1.05E+00	8.11E-02	1.22E-01	6.63E-01	1.33E+00
10	2.20E+00	1.55E+00	1.42E+00	4.73E-01	1.37E-01	3.46E+00	6.33E-01
				^{78}Sr			
0.01	5.09E-03	5.63E-03	9.04E-01	4.85E-03	2.46E-03	1.97E+00	8.14E-01
1	4.88E-03	5.66E-03	8.63E-01	4.85E-03	2.75E-03	1.76E+00	8.64E-01
2	4.78E-03	6.07E-03	7.87E-01	4.85E-03	3.35E-03	1.45E+00	9.78E-01
3	5.59E-03	7.48E-03	7.47E-01	4.85E-03	3.59E-03	1.35E+00	1.06E+00
10	5.72E-01	5.40E-01	1.06E+00	1.79E-01	4.60E-03	3.90E+01	7.25E-01

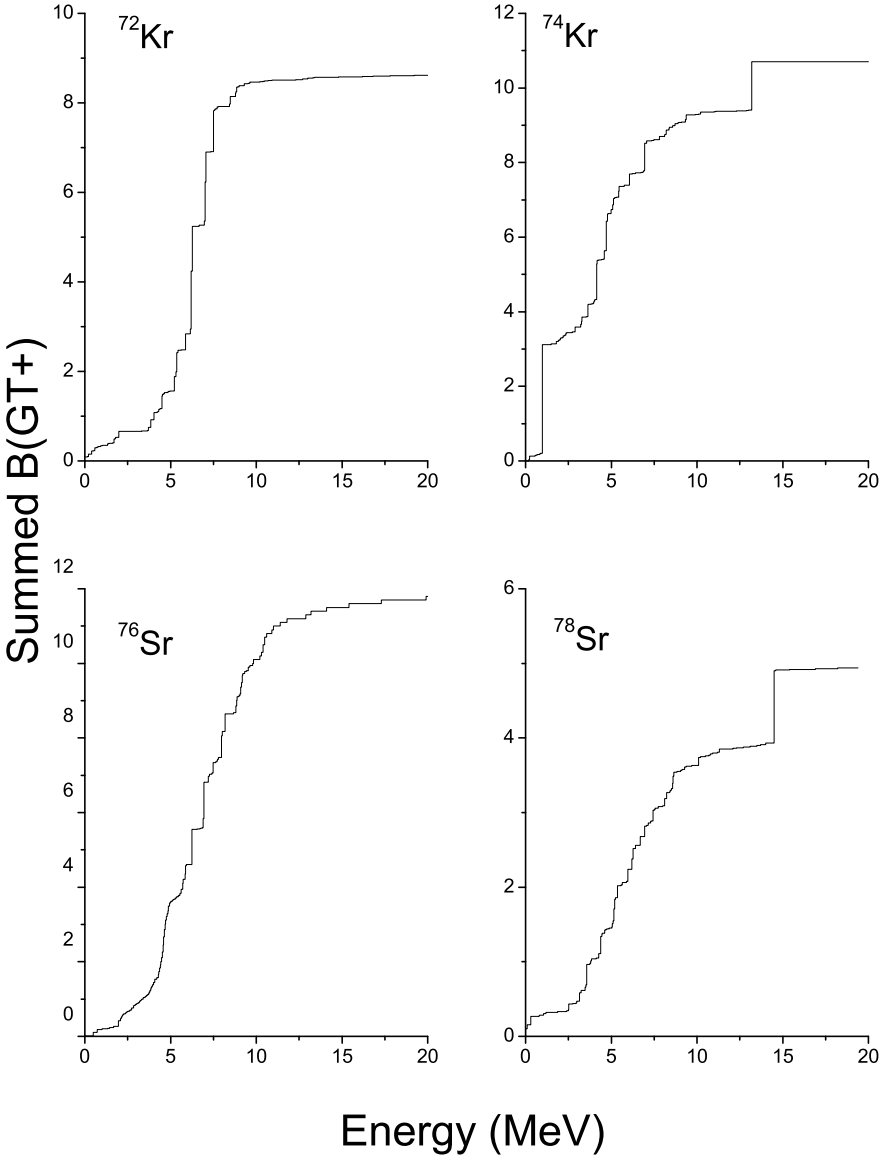

Fig. 1 Cumulated Gamow-Teller strength distributions $B(GT_+)$ for Kr and Sr isotopes. The abscissa represents energy in units of MeV in daughter nucleus.

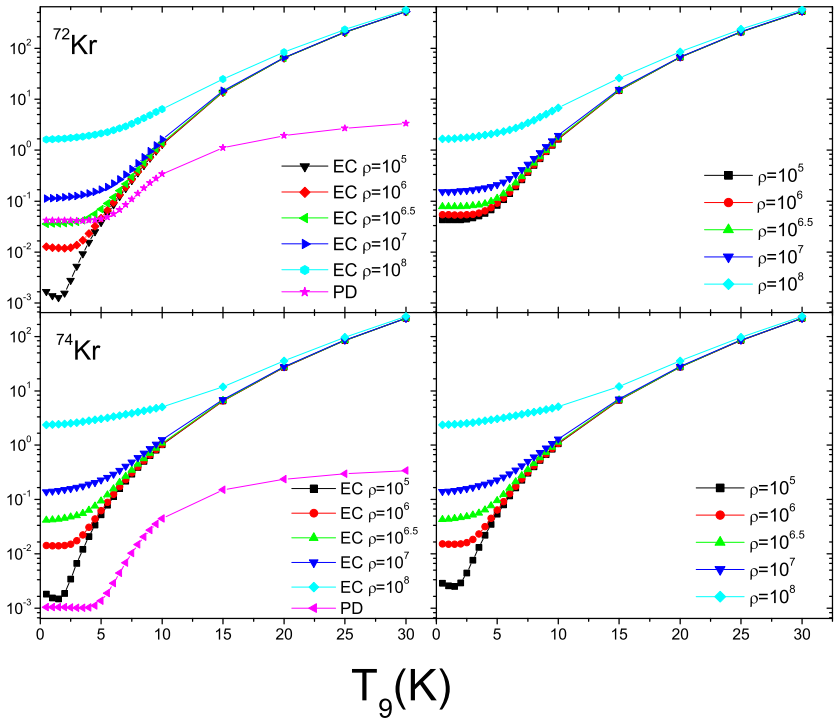

Fig. 2 (Color online) Weak-interaction mediated rates for Kr isotopes as a function of stellar temperature and density. The left panels show the electron capture and positron decay rates whereas the right panels show the combined rates. All rates are given in units of s^{-1}. Densities are given in units of gcm^{-3} and temperatures in units of 10^9 K.

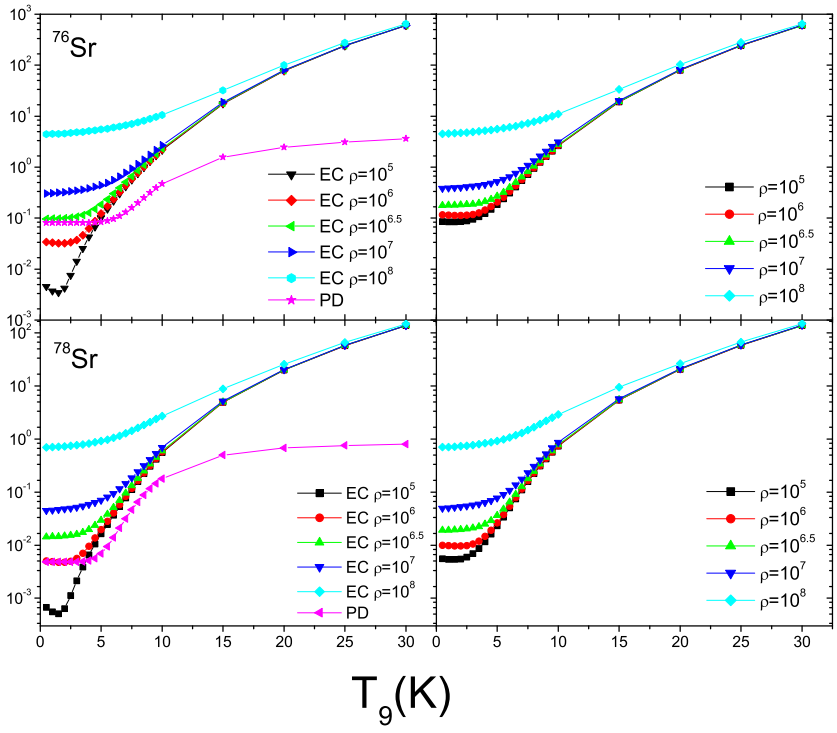

Fig. 3 (Color online) Same as Fig. 2 but for Sr isotopes.

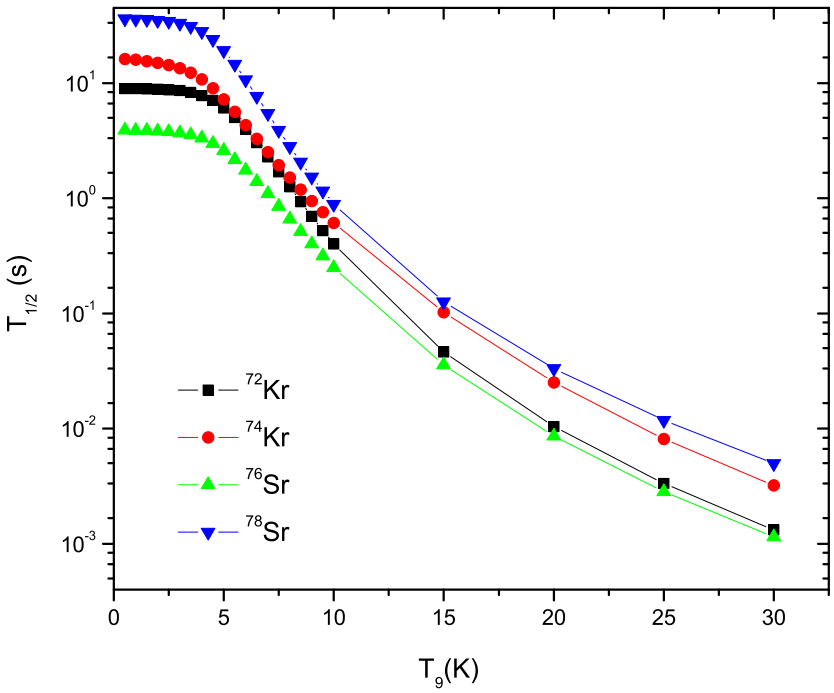

Fig. 4 (Color online) Half-lives for Kr and Sr isotopes as a function of stellar temperature calculated at a density of $\rho Y_e = 10^{6.5}$ gcm^{-3}.